Int. J. Advanced Design and Manufacturing Technology, 2022, Vol. 15, No. 4, pp. 1-12

DOI: 10.30486/admt.2023.1959626.1353 *ISSN: 2252-0406* *https://admt.isfahan.iau.ir*

Trajectory Tracking Control of a Novel Planner Continuum Robot

Seyed Shoja Amini
Department of Mechanical Engineering,
Iran University of Science and Technology, Tehran, Iran
E-mail: shjamini@gmail.com

Ali Keymasi Khalaji *
Department of Mechanical Engineering, Faculty of Engineering,
University of Kharazmi, Tehran, Iran
E-mail: keymasi@khu.ac.ir,
*Corresponding author

Received: 30 May 2022, Revised: 18 September 2022, Accepted: 23 October 2022

Abstract: Researchers have a special fondness for continuum robots (CRs) due to their various applications. CRs have been modeled in different ways. One of these methods is called lumped model. Although the lumped modeling of CRs needs multiple degrees of freedom, researchers have considered only a few degrees of freedom. But considering such structures led to some issues in the accuracy of the controller. Therefore, in this paper, the dynamic modeling of a CR which is based on the lumped model is developed in a general form. Additionally, a control strategy based on sliding mode back-stepping control is proposed after introducing the first and second Lyapunov functions for stability proof. Moreover, a new function in the control law is used to avoid chattering phenomena. The proposed controller can reduce the settling time, which is one of the most important factors in controlling such robots. To demonstrate the efficiency of the proposed method, three different case studies are conducted for a planar 8-DOF continuum manipulator and the simulations are compared with the feedback linearization method (FL). The simulations show the effectiveness of the proposed method for controlling the continuum robot.

Keywords: Feedback Linearization, Lagrange Formulation, Model-Based Control, Multi-DOF Continuum Robot, Redundancy, Sliding Mode Control

Biographical notes: Seyed Shoja Amini received his B.Sc. in Mechanical Engineering from the Islamic Azad University, North Tehran Branch in 2015 and his M.Sc. in Mechanical Engineering from Iran University of Science and Technology (IUST), Tehran, Iran in 2018. **Ali Keymasi Khalaji** received his B.Sc. from IUST, Tehran, Iran, in 2007, and his M.Sc. and Ph.D. in Mechanical Engineering from K. N. Toosi University of Technology (KNTU), Tehran, in 2009 and 2014, respectively. His research interests include modeling and control of mechanical systems, nonlinear control, adaptive and robust control with applications to mobile robotic systems, and mechatronics.

Research paper

1 INTRODUCTION

Recently, a new class of robots called continuum robots (CRs) has been introduced. These robots resemble flexible robots with many joints and degrees of freedom that allow them to adapt to and move easily in convoluted places. CRs are considered a special group inspired by some parts of animals such as octopuses, elephants or the tail of reptiles [1-4]. CRs are mainly used in medical surgery [5], e.g., in the cardiorespiratory, digestive and urogenital systems [6-9]. Although CRs have many advantages and applications, nevertheless they do not have sufficiently rigid structures, so this situation makes it hard to find a relationship between actuators and end-effector. There are some different methods for modeling CRs: classical methods [10], emerging techniques [11] and combined methods [12-13]. Although the classical methods provide an exact solution for the statics of the continuum robot, there are pitfalls in extending them to the dynamics, as this would involve the solution of a system of partial differential Equations (PDE) [14]. The PDE can represent the Equations of motion of CRs with Cosserat rod dynamics [15]. Since such Equations are so complicated, emerging techniques have been introduced. Reference [11] attempts to overcome the limitations of constant curvature modeling by replacing circular curves with Euler curves, which were found to be more suitable for a pneumatic continuum robot. Furthermore, some other methods were used in the modeling of the CRs. For instance, the backbone model is like ropes and strings with infinite degrees of freedom. Mochiyama and Suzuki, using the Frenet-Serret formulas, could approximate the kinematics and dynamics of such a model [16]. Yoon and Yi designed a flexible 4-DOF robot, cable-driven CRs, consisting of two modules with a backbone spring [17]. This model was imitated from the biological backbone and its main goal was considering collision avoidance. In another research, the Equations of motion of planar continuum manipulators were extracted by Tatlicioglu et all. considering the effects of potential energy. However, this model has not been experimentally validated [18]. The control of CRs can be divided into three different types. The first would be kinematic control [19]. This method uses a forward and inverse kinematic modeling of the system. The second type is the feedforward position control strategy which is based on a Piecewise Constant Curvature hypothesis. This method improved the robustness against disturbances of the system [20-21]. The third one is differential kinematics, which is partially effective for redundant manipulators because it allows multi-task control [22]. However, this method requires some assumptions that reduce the accuracy of the system. To address this problem, adaptive and learning approaches have been introduced by some researchers. These approaches are based on data gathering [23]. In another study, the authors proposed an observer control based on Youla parameterization for a flexible link with the lumped tip mass [24-25]. The idea of this method was based on the using Youla parameter instead of finding the transfer function. But, the limitation of this method is that the dynamics Equations should be linearized.

There are many challenges in modeling CRs because the structure has an unlimited number of degrees of freedom, which makes the formulation very complex. For this reason, researchers have considered limited degrees of freedom in modeling based on a lumped model [26]. However, modeling and control of CRs require accurate dynamic models. To improve the efficiency of dynamic modeling and the difficulties mentioned in the previous paragraph, this paper extracts the kinematic and dynamic Equations in general form through the Lagrangian formulation. In addition, the accurate position control of the end-effector by the sliding mode back-stepping control (SMBSC) method is investigated. The accuracy and speed in controlling this type of robot are crucial in surgical and medical applications. By introducing such a controller, not only is the error negligible but also the settling time decreases sharply. This paper is organized as follows. In the first section, the dynamic modeling of this robot is presented and the Equations of motion of this system are developed using the Lagrangian formulation. Section 2 explains the formulation of SMBSC. Section 3 shows how to linearize a nonlinear system using the input-output with the feedback linearization method. Simulation using MATLAB software is presented in section 4. Section 5 contains the conclusion of the paper.

2 MODELING

One model of CRs comprises a 2n degrees of freedom arm which is demonstrated in "Fig. 1". The idea of this model was obtained from [26]. System dynamic is obtained with Lagrange method:

$$\frac{d}{dt}\left(\frac{\partial L}{\partial \dot{q}}\right)-\left(\frac{\partial L}{\partial q}\right)+\left(\frac{\partial D}{\partial \dot{q}}\right)=Q \tag{1}$$

Where, L represents the kinetic energy minus potential energy of the system. In addition, Q is the vector of generalized forces. The Equations of motion are demonstrated as:

$$\begin{aligned}&[I]_{2n\times 2n}[\ddot{q}]_{2n\times 1}+[C]_{2n\times 1}+[G]_{2n\times 1}=[u]_{2n\times 1}+[d]_{2n\times 1}\\ &,\\ &q=[s_1,s_2,...,s_n,\theta_1,\theta_2,...,\theta_n]^T\\ &u=\left[F_1,F_2,F_3,F_4,...,F_{(2n-1)},F_{2n}\right]^T\end{aligned} \tag{2}$$

Where I demonstrates mass matrix which is symmetric positive definite, C (q, q □) represents the forces of centrifugal and Coriolis force, G(q) is the gravity vector and u(t) is the vector of inputs which include the forces acting on the springs and dampers. In the given Equation, q shows the generalized coordinates, d(t) is the torque that expresses finite disturbance, modelling uncertainties, and unmodulated dynamics.

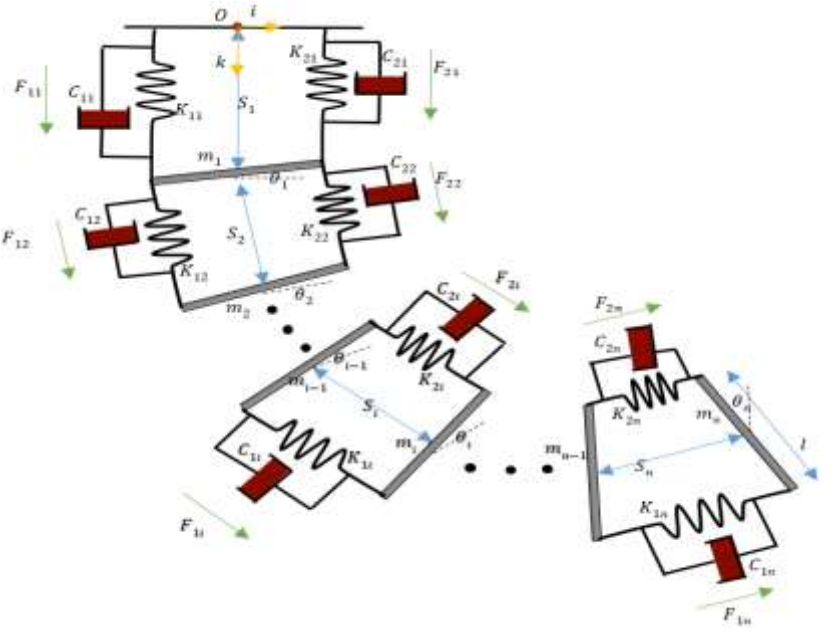

Fig. 1 Continuum robot manipulator via springs and dampers structure.

3 SLIDING MODE BACK-STEPPING CONTROL

In this section, an SMC law for the convergence of robot variables to optimal values is designed. Robust nonlinear SMC control is an effective technique and its applications have greatly increased in recent decades.
The most important feature of SMC is insensitivity to changes and disturbances in system parameters and external disturbances. In addition, it provides a fast-passing response. In the SMC method proposed in this section, by back stepping design, sliding switching plates are introduced, and then, this rule is designed for asymptotic stability of the closed-loop error system. In general, conventional SMC does not have the desired ability to control the system due to the sign (σ) function;
Because the existence of the sign function due to discontinuity around zero, causes the phenomenon of chattering, which is sharp fluctuations around the equilibrium point of error at zero. It is worth mentioning that this problem is considered in the design of the control law.

System description
The first step in designing an SMC law is to define the appropriate sliding plates. But, before that, and in order to start the design process, first the state space of this CR is considered.

$$\begin{aligned} x_1(t) &= q(t) \\ x_2(t) &= \dot{q}(t) \end{aligned} \tag{3}$$

The robot dynamic Equations can be written as follows:

$$\begin{aligned} \dot{x}_1(t) &= x_2(t) \\ \dot{x}_2(t) &= [I]^{-1}_{2n\times 2n}\left\{[u]_{2n\times 1}+[d]_{2n\times 1}-[C]_{2n\times 1}-[G]_{2n\times 1}\right\} \end{aligned} \tag{4}$$

In fact, in the SMBSC method, according to the control diagram showing in the “Fig. 2”, the switching plates are designed in such a way that after applying the controller, the time Equation of this plate and its derivative becomes zero, and when they become zero, the system modes also converge to zero. For this purpose, sliding plates are defined as follows [27].

$$\sigma_i = x_i - \alpha_{i-1} \quad i = 1,2 \tag{5}$$

Where, $\alpha_0 = x_{1d}$ shows the optimal value for x_1, σ_i represents the sliding plate vector, and α_i represents the ideal state vector for x_i and is an intermediate value.

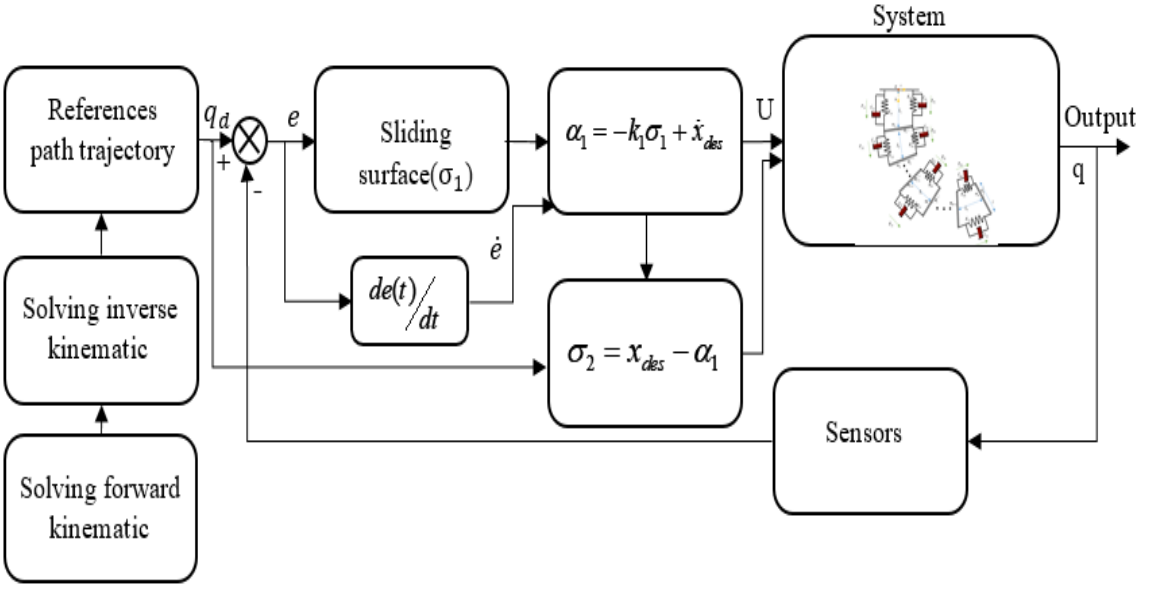

Fig. 2 SM control structure diagram.

Designing sliding mode back-stepping control

The design of the control law in this section will be done in two steps. In the first step, virtual control input is designed and then, the control law will be performed to stabilize the whole design system and prove its stability through Lyapunov. In the first stage, the first subsystem in modeling is the Equation $\dot{x}_1 = x_2$ in which x_2 is a virtual input for this system and the derivative of the first sliding plate ($\sigma_1 = x_1 - x_{1d}$) with respect to time is:

$$\dot{\sigma}_1 = \dot{x}_1 - \dot{x}_{1d} = x_2 - \dot{x}_{1d} \tag{6}$$

On the other hand, according to "Eq. (5)", $\sigma_2 = x_2 - \alpha_1$ and by placing x_2 in "Eq. (6)":

$$\dot{\sigma}_1 = \dot{x}_1 - \dot{x}_{1d} = x_2 - \dot{x}_{1d} = \sigma_2 + \alpha_1 - \dot{x}_{1d} \tag{7}$$

In order to converge the first subsystem to the sliding plate and move on it, the virtual control rule is defined as follows:

$$\alpha_1 = -k_1\sigma_1 + \dot{x}_{1d} \tag{8}$$

Where: $k_1 > 0$.

Now, the first Lyapunov function is considered as follows:

$$V_1 = \frac{1}{2}\sigma_1^T\sigma_1 \tag{9}$$

By calculating the derivative of the Lyapunov function ("Eq. (9)") and placing "Eq. (7)" and "Eq. (8)" in it, "Eq. (10)" is obtained:

$$\dot{V}_1 = \sigma_1^T\dot{\sigma}_1 = -k_1\|\sigma_1\|^2 + \sigma_1^T\sigma_2 \tag{10}$$

In the second stage, the second sliding plate is $\sigma_2 = x_2 - \alpha_1$. The derivative of the second sliding surface with respect to time would be as "Eq. (11)". The "Eq. (4)" and "Eq. (7)" are used as follow:

$$\begin{aligned}&\dot{\sigma}_2 = \dot{x}_2 - \dot{\alpha}_1\\ &= I^{-1}(x)[-C(x_1,x_2) - G(x) + u(t) + d(t)]\\ &+k_1\dot{\sigma}_1 - \ddot{x}_{1d} = I^{-1}(x)[-C(x_1,x_2) - G(x) + u(t) + d(t)]\\ &+k_1(\sigma_2 + \alpha_1 - \dot{x}_{1d}) - \ddot{x}_{1d}\end{aligned} \tag{11}$$

With the following definitions:

$$\begin{aligned}&f(x_1,x_2) \triangleq I^{-1}(x)[-C(x_1,x_2) - G(x)]\\ &+k_1(\sigma_2 + \alpha_1 - \dot{x}_{1d}) - \ddot{x}_{1d}\\ &g \triangleq I^{-1}(x)\end{aligned} \tag{12}$$

According to the "Eq. (12)", "Eq. (11)" is obtained as follows:

$$\dot{\sigma}_2 = f(x_1,x_2) + gu(t) + gd(t) \tag{13}$$

Now the control law is proposed as follows:

$$u(t) = g^{-1}\left\{-f(x_1, x_2) - k_2\sigma_2 - \sigma_1 - \bar{d}\,\|g\|\mathrm{si}\,gn(\sigma_2)\right\} \quad (14)$$

By placing "Eq. (14)" in "Eq. (13)":

$$\dot{\sigma}_2 = -k_2\sigma_2 - \sigma_1 - \bar{d}\,\|g\|\mathrm{si}\,gn(\sigma_2) + gd(t) \quad (15)$$

By considering the Lyapunov function:

$$V_2 = V_1 + \frac{1}{2}\sigma_2^T\sigma_2 \quad (16)$$

The derivative of the Lyapunov function with respect to time becomes as "Eq. (17)". In this Equation, "Eq. (10)" has been utilized.

$$\dot{V}_2 = \dot{V}_1 + \sigma_2^T\dot{\sigma}_2 = -k_1\|\sigma_1\|^2 + \sigma_1^T\sigma_2 + \sigma_2^T\dot{\sigma}_2 \quad (17)$$

By placing the derivative of second sliding plate ("Eq. (15)") in "Eq. (17)":

$$\begin{aligned}\dot{V}_2 &= \dot{V}_1 + \sigma_2^T\dot{\sigma}_2\\ &= -k_1\|\sigma_1\|^2 + \sigma_1^T\sigma_2\\ &+\sigma_2^T(-k_2\sigma_2 - \sigma_1 - \bar{d}\,\|g\|\mathrm{si}\,gn(\sigma_2) + gd(t))\\ &= -k_1\|\sigma_1\|^2 + \sigma_1^T\sigma_2 - k_2 gd(t)\end{aligned} \quad (18)$$

The expressions ${\sigma_1}^T\sigma_2$ is transpose of ${\sigma_2}^T\sigma_1$ and are therefore equaled and deleted with each other.

$$\begin{aligned}\dot{V}_2 &= -k_1\|\sigma_1\|^2 - k_2\|\sigma_2\|^2 - \bar{d}\,\|g\|\sigma_2^T\,\mathrm{si}\,gn(\sigma_2)\\ &+\sigma_2^T gd(t) = -k_1\|\sigma_1\|^2 - k_2\|\sigma_2\|^2 - \bar{d}\,\|g\|\|\sigma_2\|\\ &+\sigma_2^T gd(t) \le -k_1\|\sigma_1\|^2 - k_2\|\sigma_2\|^2 - \bar{d}\,\|g\|\|\sigma_2\|\\ &+\|\sigma_2\|\|g\|\|d(t)\|\\ &= -k_1\|\sigma_1\|^2 - k_2\|\sigma_2\|^2 + (\|d(t)\| - \bar{d})\|\sigma_2\|\|g\| < 0\end{aligned} \quad (19)$$

On the other hand, according to the assumption $\|d(t)\| \le \bar{d}$ where $\bar{d} \in R^+$, the Equation $\|d(t)\| - \bar{d} \le 0$ is gained and consequently $\dot{V}_2 < 0$. Therefore, the $\dot{V}$ is negative for all values of σ, and as a result, according to the definition of sliding plates and Lyapunov's theorem, it can be concluded that when the sliding plate becomes zero, the error value converges to zero and finally $x_1 \to x_{1d}$.

Improving the discontinuity in the controller

In the controller expressed in "Eq. (14)", the sign function with a coefficient in the Equation is used. The sign function $u = \bar{d}sign(\sigma)$, which can also be expressed as: $u = \bar{d}\,\sigma/\|\sigma\|$, is a discontinuous function around σ = 0. This discontinuity in the law of control can provide difficulty and cause a phenomenon called chattering. This phenomenon causes fluctuations in the input value of the robot system, especially when the system is exposed to noise. To counteract the chattering phenomenon, the value of u in the control law must be changed. To address this issue, proposals such as using $\tanh(\sigma)$ or saturation function (sat (σ)) instead of $\sigma/\|\sigma\|$ have been suggested. However, another idea is used in this paper. Due to the fact that this discontinuity occurs when σ convergences to zero, the best choice to prevent discontinuities and unevenness in u is to add a term and consider it as follows:

$$u = \frac{\bar{d}^2\sigma}{\bar{d}\,\|\sigma\| + \Gamma(t)} \quad (20)$$

Where, Γ(t) is a positive function such that $\int_0^\infty \Gamma(t)dt < \infty$ (tends to zero over time). By selecting the sign function in the control law as "Eq. (20)", the obstacle of discontinuity in the control law will be solved. The choice of this function is arbitrary and for example one of the options can be as follows:

$$\Gamma(t) = \frac{1}{1+t^n}\ , n \ge 2 \quad (21)$$

It should be noted that when Γ(t) becomes zero, the value of u in "Eq. (20)" will be similar to the $\rho\,\sigma/\|\sigma\|$.

4 FEEDBACK LINEARIZATION CONTROL BY INPUT-OUTPUT METHOD

In this method, nonlinear system dynamics transform into a (fully or partly) linear one, so that linear control techniques can be applied. First of all, we have to generate a direct relationship between the output y(t) and the input u(t). By taking two differentiations, the control input will appear to the output of this system and accordingly the relative degree of each of the outputs is equal to 2. It is obvious that if the control input never appears after more than n differentiations, the system would not be controllable. Also, in some cases, internal dynamics must be studied. Since the number of inputs and outputs are the same in this system, there is no internal dynamics. Also, it is indispensable to define a suitable output vector describing the system's attitude properly. The output of the system is all generalized coordinates and is defined as "Eq. (22)":

$$y = [s_1, s_2, ..., s_n, \theta_1, \theta_2, ..., \theta_n] \quad (22)$$

Then, according to the Equations of motion governing the system, the new input of the system is equaled to:

$$[\upsilon]_{2n\times1} = [\ddot{q}]_{2n\times1} = [I]^{-1}_{2n\times2n}\left\{-[C]_{2n\times1} - [G]_{2n\times1} + [u]_{2n\times1} + [d]_{2n\times1}\right\} \quad (23)$$

The state-space representation of the system is:

$$\dot{x} = \frac{d}{dt}\begin{bmatrix}[q]\\ [\dot{q}]\end{bmatrix} = \begin{bmatrix} \dot{s}_1 \\ \dot{s}_2 \\ \vdots \\ \dot{s}_n \\ \dot{\theta}_1 \\ \dot{\theta}_2 \\ \vdots \\ \dot{\theta}_n \\ ------ \\ [I]^{-1}_{2n\times2n}\left\{-[C]_{2n\times1} - [G]_{2n\times1} + [u]_{2n\times1} + [d]_{2n\times1}\right\} \end{bmatrix}_{4n\times1} \quad (24)$$

In this part, u must be selected in such a way as to eliminate the nonlinear terms of the system. Therefore, according to "Eq. (23)", "Eq. (25)" is obtained:

$$[u]_{2n\times1} = [I]_{2n\times2n}[\upsilon]_{2n\times1} + [C]_{2n\times1} + [G]_{2n\times1} - [d]_{2n\times1} \quad (25)$$

The following form of "Eq. (24)" is converted to "Eq. (26)":

$$\dot{x} = \begin{bmatrix}[0]_{(2n\times2n)} & [I]_{(2n\times2n)}\\ [0]_{(2n\times2n)} & [0]_{(2n\times2n)}\end{bmatrix}[x] + \begin{bmatrix}[0]_{(2n\times2n)}\\ [I]_{(2n\times2n)}\end{bmatrix}[\upsilon] \in 4n\times1$$
$$y = [[I]_{(2n\times2n)} \quad [0]_{(2n\times2n)}][x] \in 2n\times1 \quad (26)$$

5 NUMERICAL SIMULATION IN MATLAB

In this section, the model proposed in the first section is considered. This continuum robot contains four masses of rigid rod and eight springs and dampers. The generalized coordinates are chosen as:

$$q = [s_1, s_2, s_3, s_4, \theta_1, \theta_2, \theta_3, \theta_4]^T \quad (27)$$

The dynamic characteristics of the robot are presented in the following "Table 1". In the following, three different cases are considered.

Table 1 The dynamic characteristics of continuum robot

parameters	value	unit
M_i	$M_1 = 0.2$; $M_2 = 0.15$; $M_3 = 0.15$; $M_4 = 0.1$	Kg
I_i	$I_1 = I_2 = I_3 = I_4 = 0.001$	$Kg.m^2$
k_i	$k_{11} = 30$; $k_{12} = 25$; $k_{13} = 15$; $k_{14} = 15$ $k_{21} = 30$; $k_{22} = 25$; $k_{23} = 15$; $k_{24} = 15$	$N.m^{-1}$
c_i	$c_{11} = c_{12} = c_{13} = c_{14} = 10$ $c_{21} = c_{22} = c_{23} = c_{24} = 10$	$N.s.m^{-1}$
S_{0i}	$S_{01} = S_{01} = 0.2$; $S_{03} = S_{04} = 0.15$	m
l	$l = 0.2$	m
g	$g = 9.81$	$N.kg^{-1}$

Case study 1: point-to-point control design

In this subsection, point-to-point controller with SMC and FL is considered. The start and end points of the point-to-point motion are considered as $p_i(0.3, 0.25, 0.2, 0.15)$ and $p_f(0.4, 0.35, 0.3, 0.25)(m)$, respectively. The initial and desired angles are $(0.15, 0.1, 0.05, 0.05)$ and $(0.25, 0.2, 0.1, 0.1)(rad)$, respectively. The results of simulation are shown in "Fig. 3" to "Fig. 9". Figure 3 and "Fig. 4" display the time varying changes of the extension of each module with FL and SMS methods. It is observed that state variables start from their initial conditions and finally reach to their final positions. All the states with SMC method reach their desired values way sooner. Figure 5 and "Fig. 6" represent the change in orientation of the rigid rod angles starting from their initial conditions to their final positions.

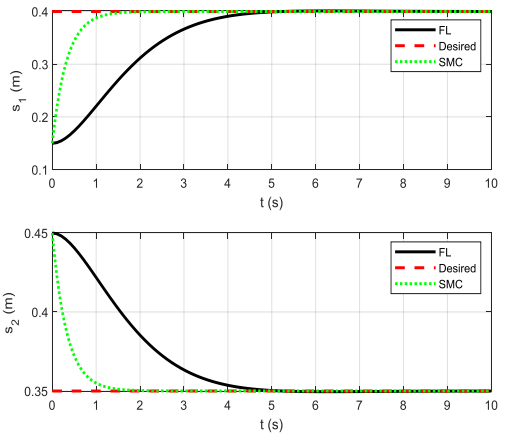

Fig. 3 The time varying changes of parameter s_1 and s_2.

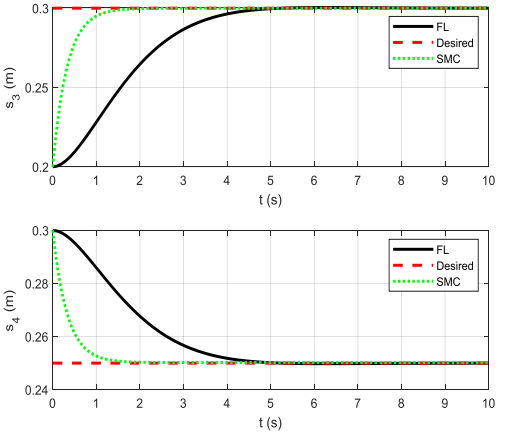

Fig. 4 The time varying changes of parameter s_1 and s_4.

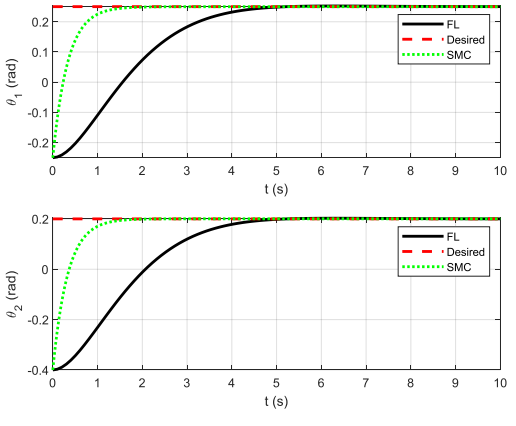

Fig. 5 The change in orientation of the rigid rod (θ_1, θ_2).

In "Fig. 7", the trajectory of the end-effector of robot is shown. The structures of the robot in initial and desired points are demonstrated too. In "Fig. 8" and "Fig. 9", the amount of inputs is indicated.

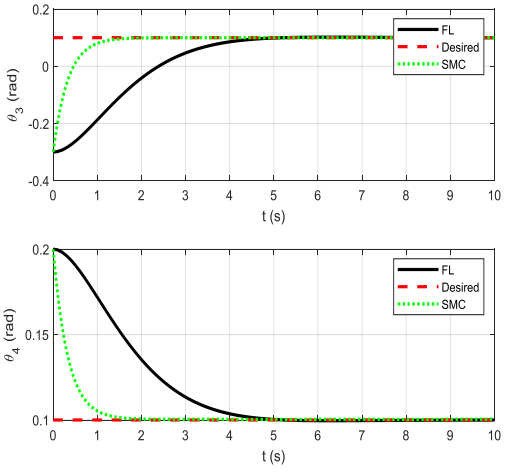

Fig. 6 The change in orientation of the rigid rod (θ_3, θ_4).

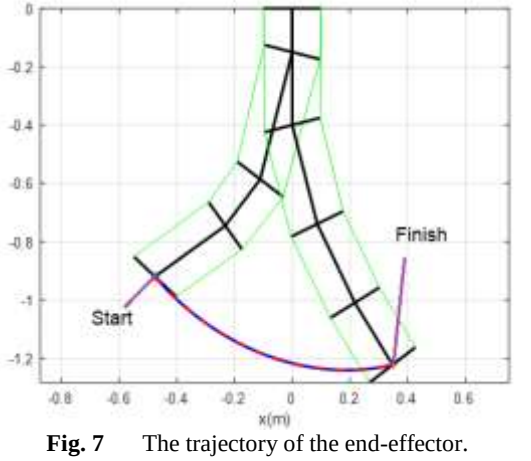

Fig. 7 The trajectory of the end-effector.

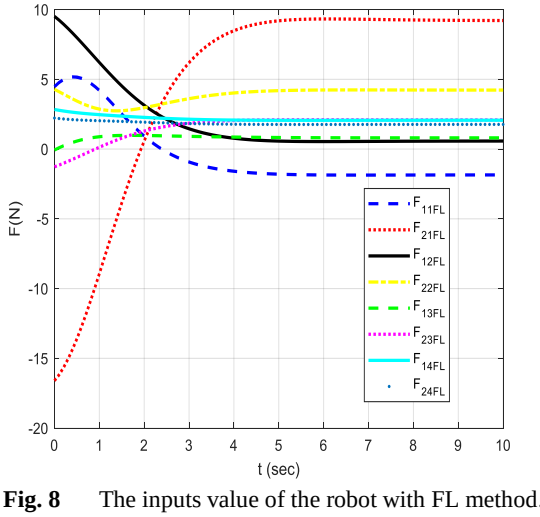

Fig. 8 The inputs value of the robot with FL method.

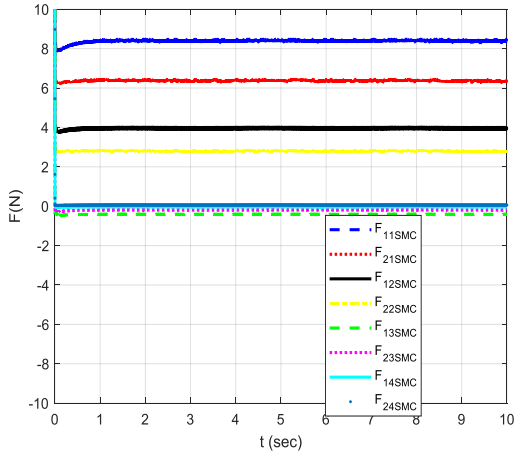

Fig. 9 The inputs value of the robot with SMC method.

According to the input diagram, it is clear that in the FL method, initially, the amount of inputs changes until states reach their references. But, over time these inputs reach fixed values at the end of the path. Due to the fact that the dynamic model of the system has gravitational acceleration, the values of the inputs cannot reach zero. Also, according to the diagrams of the SMC method, it can be seen that in this method states reach their desired value sooner so inputs show the stable trend.

Case study 2: point-to-point control design with disturbances

In this part, some disturbances between 1.5 and 2.5 seconds are introduced to this system. As well as this, all parameters and dimensions of the robot remain unchanged. The target of this case study is to examine the performance of the controllers despite the disturbance. Figure 10 and Fig. 11" illustrate the time-varying changes of the extension of each module with FL and SMS methods.

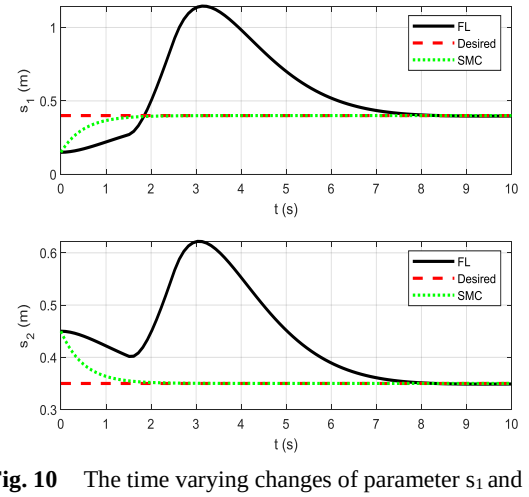

Fig. 10 The time varying changes of parameter s_1 and s_2.

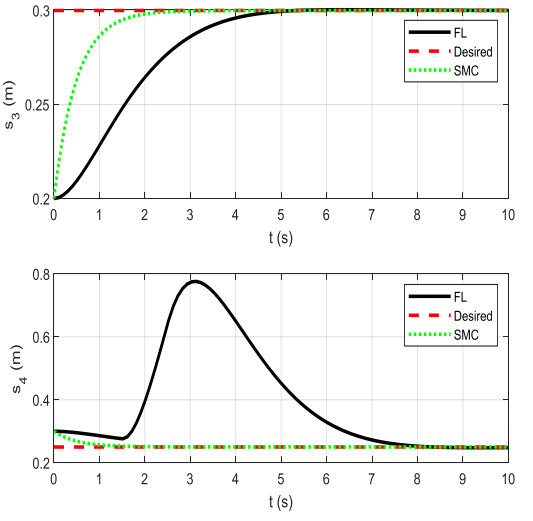

Fig. 11 The time varying changes of parameter s_1 and s_4.

It can be seen that before the time when the disturbances are applied, FL controller tries to reach desired points. But, when figures with FL method reach the time when there are disturbances, their states move away from the desired values. After this period, the controller tries to revise this situation and reach references. On the other hand, these disturbances have little effect on the system with SMC method. Figure 12 and "Fig. 13" represents the change in orientation of the rigid rod angles starting from their initial conditions to their final positions. The trajectory of the end-effector of the robot is indicated in "Fig. 14".

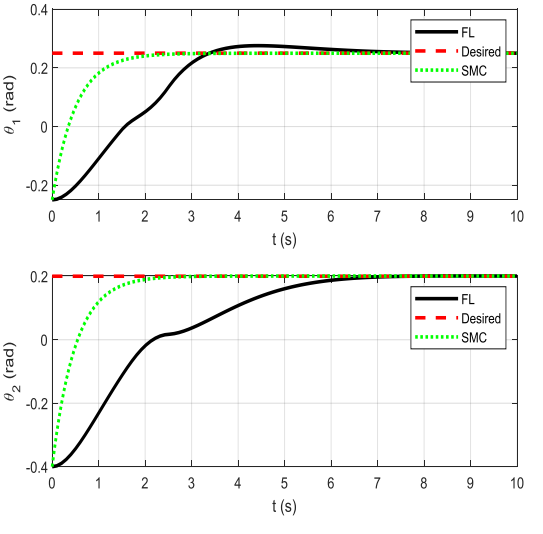

Fig. 12 The change in orientation of the rigid rod(θ_1, θ_2).

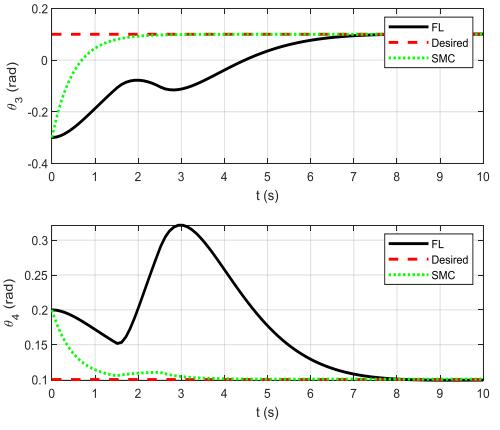

Fig. 13 The change in orientation of the rigid rod(θ_3, θ_4).

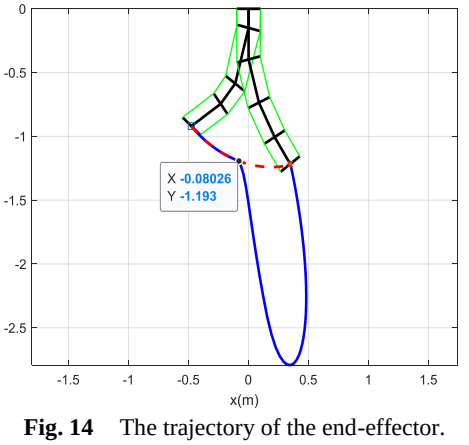

Fig. 14 The trajectory of the end-effector.

The end-effector of the robot until 1.5 seconds (before disturbance time) reaches (-0.08, -1.19) location. When disturbance starts, the trajectory of the end-effector changes. In the simulation, it is shown that the robot's path remains unchanged after 4.93 seconds. To be more exact the end-effector reaches the endpoint. In "Fig. 15" and "Fig. 16", the amount of inputs with disturbances are presented.

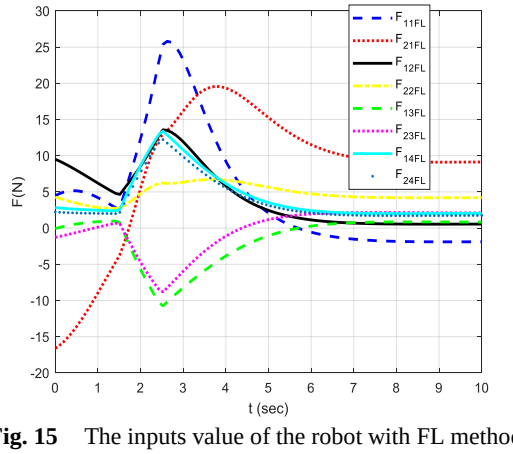

Fig. 15 The inputs value of the robot with FL method.

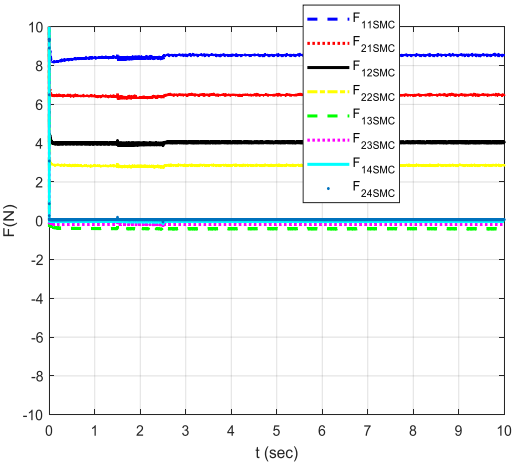

Fig. 16 The inputs value of the robot with SMC method.

According to the input diagram, it is clear that after 1.5 seconds many changes are made in the input charts in the FL method. Compared to the input diagrams in "Fig. 8", the power input changes of force F_{11} are significant. But as it turns out, after 6 seconds it reaches the same input values of the form without disturbance. Moreover, the least change is related to force F_{22}. The main justification for this trend is the small effects of disturbance on the S_3, θ_1 *and* θ_2 variables according to the pattern of "Fig. 11" and "Fig. 12". Likewise, "Fig. 9", the disturbances had little effect on the input diagrams in "Fig.16". Therefore, the SMC controller has better performance.

Case study 3: Circular trajectory design

The desired trajectory selected is a circular path on the plane that needs to be followed by the end-effector. Therefore, this path is assumed to be as follow:

$$\begin{pmatrix} x_{des} & z_{des} \end{pmatrix} = \begin{pmatrix} \cos(2t) & \sin(2t) \end{pmatrix} \quad (28)$$

For this purpose, it is necessary to solve the inverse kinematics to find the desired values of the variables q. The forward kinematic Equations of the robot, which expresses the location of the end-effector is:

$$\begin{aligned} x &= s_2 \sin(\theta_1) + s_3 \sin(\theta_1 + \theta_2) + s_4 \sin(\theta_1 + \theta_2 + \theta_3) \\ z &= s_1 + s_2 \cos(\theta_1) + s_3 \cos(\theta_1 + \theta_2) \\ &+ s_4 \cos(\theta_1 + \theta_2 + \theta_3) \\ \theta &= \theta_1 + \theta_2 + \theta_3 + \theta_4 \end{aligned} \quad (29)$$

Due to the fact that there are 8 variables and the number of variables required to follow a circular path is 2 variables; Therefore, inverse kinematics will definitely have countless answers. To solve it, we give the value of 6 variables:

$$\theta_1=\frac{\pi}{10},\theta_2=\frac{\pi}{8},\theta_3=\frac{\pi}{5},\theta_4=\frac{\pi}{6},s_1=0.3,s_2=0.4 \qquad (30)$$

By placing the values of "Eq. (30)" in the robot kinematic Equation in "Eq. (29)", the other two variables, s_3 and s_4, are obtained as follows:

$$\begin{aligned} s_3 &= 1.65\sin 2t - 0.39\cos 2t - 1.07 \\ s_4 &= 1.29\cos 2t - 1.11\sin 2t + 0.59 \end{aligned} \qquad (31)$$

Therefore, the desired values for q_{des} are selected according to the definition of q ("Eq. (27)"). Besides, the initial condition of the system is demonstrated as:

$$p_{initial}=\left[-1;0.8;1.2;0.3;0.5;0.1;0.2;0.7\right] \qquad (32)$$

In the following, "Fig. 17" to "Fig. 20" show the diagrams of the output systems of the system consisting of 8 variables along with the desired references with FL and SMS methods. The error of all 8 state variables with SMC becomes zero in less than 0.5 seconds, and this is a sign of the high speed of the designed controller.

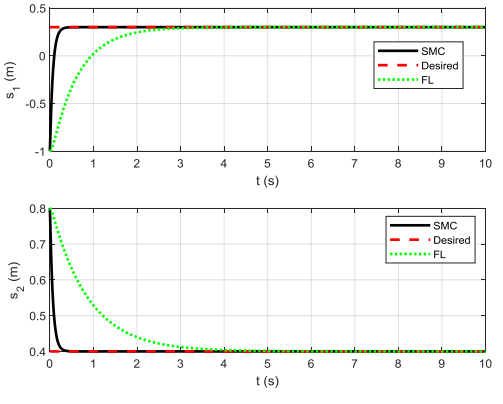

Fig. 17 The time varying changes of parameter s_1 and s_2.

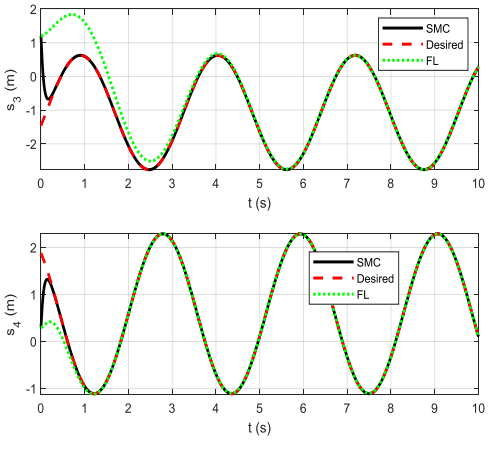

Fig. 18 The time varying changes of parameter s_3 and s_4.

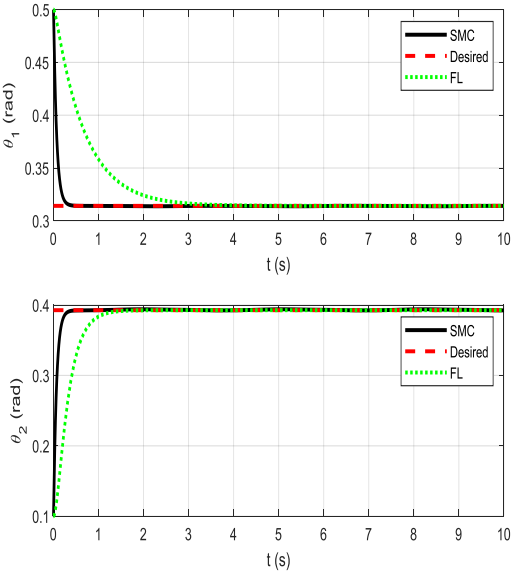

Fig. 19 The change in orientation of the rigid rod (θ_1,θ_2).

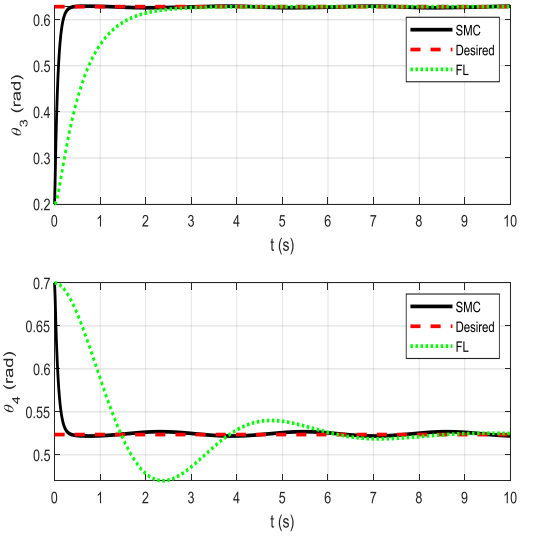

Fig. 20 The change in orientation of the rigid rod (θ_3,θ_4)

According to the results of inverse kinematics in "Eq. (31)", the desired path for the variables s_3 and s_4 is in the form of trigonometric functions shown in "Fig. 18". Besides, by placing the expression t=0 in "Eq. (31)", the initial values of the mentioned variables are calculated. In "Fig. 21", the trajectory of the end-effector of the robot in the 2-D plane is illustrated.

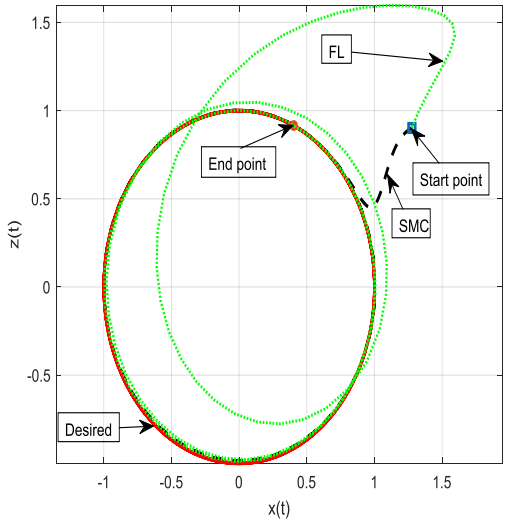

Fig. 21 The trajectory of the end-effector.

In "Fig. 21", the end-effector starts from the initial point which has been shown. This point is calculated with forward kinematic which was represented in "Eq. (29)". For calculation of the initial point of the path, all 8 variables are needed. Such parameters were calculated in "Eq. (30)" and "Eq. (31)". This point would be (1.276, 0.915). Similar to this approach, the final point would be (0.3447, 0.9429).

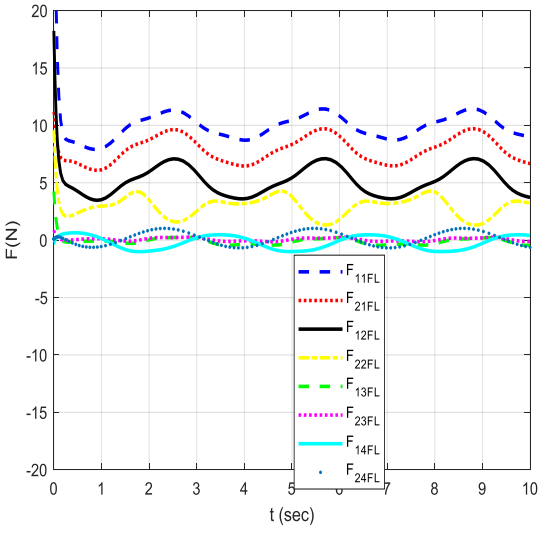

Fig. 22 The inputs value of the robot with FL method.

In addition, the path traveled by SMC method has less mean squared error than FL method. It is seen that, even though both FL and SMC methods have the same dynamic modeling, controllers trace the different paths during the beginning and circular path. The factor of these two paths is the FL approach. In "Fig. 22" and "Fig. 23", the amount of inputs is shown. Now See "Table 2".

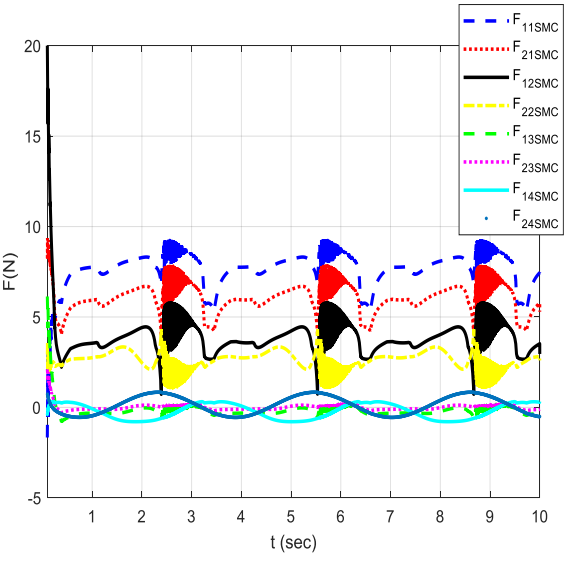

Fig. 23 The inputs value of the robot with SMC method.

Table 2 The comparison between tacking error with SMC and FL methods

Control Method	Mean Squared Error(m^2)
SMC	0.004
FL	0.245

It should be noted that even though the inputs by FL method is higher than SMC method, the trajectory of the end-effector in "Fig. 21" reaches the desired path with SMC method much sooner.

6 CONCLUSIONS

This paper presents a novel nonlinear control law for multi-DOF discrete CR. The dynamic model is based on a new structure established recently. However, in this work, the model of the system is developed into general form. Moreover, the strategy of SMC for a CR was presented in this paper with the stability proof of the system with Lyapunov theory. Besides, control simulation for three different cases was presented with SMC and the results were compared with the input-output feedback linearization method in MATLAB software. The results exhibited that the settling time of the former method is much lesser than the latter approach. It should be noted that the proposed control model can be presented in various applications, including the medicine, where the rapid control of the CRs is so important.

REFERENCES

[1] Hyatt, P., Johnson, C. C., and Killpack, M. D., Model Reference Predictive Adaptive Control for Large-Scale Soft Robots, Frontiers in Robotics and AI, 2020, pp. 558027.

[2] Hsiao, J. H., Chang, J. Y., and Cheng, C. M., Soft Medical Robotics: Clinical and Biomedical Applications, Challenges, and Future Directions, Advanced Robotics, Vol. 33, No. 21, 2019, pp. 1099-1111.

[3] Yeshmukhametov, A., et al. Modeling and Validation of New Continuum Robot Backbone Design with Variable Stiffness Inspired from Elephant Trunk, IOP Conference Series: Materials Science and Engineering, Vol. 417, No. 1, 2018, pp. 012010.

[4] Zheng, Z., et al., Dynamic Analysis of Elastic Projecting Robot Inspired by Chameleon Tongue, IEEE International Conference on Robotics and Biomimetics (ROBIO), 2018, Dec 12, pp. 2088-2094.

[5] Simaan, N., et al., Design and Integration of a Telerobotic System for Minimally Invasive Surgery of The Throat, The International Journal of Robotics Research, Vol. 28, No. 9, 2009, pp. 1134-1153.

[6] Da Veiga, T., et al., Challenges of Continuum Robots in Clinical Context: A Review, Progress in Biomedical Engineering, Vol. 2, No. 3, 2020, pp. 032003.

[7] Ahmad, M. A., et al., Deep Learning-Based Monocular Placental Pose Estimation: Towards Collaborative Robotics in Fetoscopy, International Journal of Computer Assisted Radiology and Surgery, Vol. 15, No. 9, 2020, pp. 1561-1571.

[8] Shi, C., et al., Shape Sensing Techniques for Continuum Robots in Minimally Invasive Surgery: A Survey. IEEE Transactions on Biomedical Engineering, Vol. 64, No. 8, 2016, pp. 1665-1678.

[9] Sarli, N., et al., Preliminary Porcine In Vivo Evaluation of A Telerobotic System for Transurethral Bladder Tumor Resection and Surveillance, Journal of Endourology, Vol. 32, No. 6, 2018, pp. 516-522.

[10] Webster, R., B. A. Jones, Design and Kinematic Modeling of Constant Curvature Continuum Robots: A review, The International Journal of Robotics Research, Vol. 29, No. 13, 2010, pp. 1661-1683.

[11] Gonthina, P. S., et al., Modeling Variable Curvature Parallel Continuum Robots Using Euler Curves, International Conference on Robotics and Automation (ICRA), 2019, May 20, pp. 1679-1685.

[12] Rone, W. S., Ben-Tzvi, P., Mechanics Modeling of Multisegment Rod-Driven Continuum Robots, Journal of Mechanisms and Robotics, Vol. 6, No. 4, 2014, pp. 041006.

[13] Kratchman, L. B., et al., Guiding Elastic Rods with A Robot-Manipulated Magnet for Medical Applications, IEEE Transactions on Robotics, Vol. 33, No. 1, 2016, pp. 227-233.

[14] Till, J., Aloi, V., and Rucker, C., Real-Time Dynamics of Soft and Continuum Robots Based on Cosserat Rod Models, The International Journal of Robotics Research, Vol. 38, No. 6, 2019, pp. 723-746.

[15] Sadati, S. H., et al., TMTDyn: A Matlab Package for Modeling and Control of Hybrid Rigid–Continuum Robots Based on Discretized Lumped Systems and Reduced-Order Models, The International Journal of Robotics Research, Vol. 40, No. 1, 2021, pp. 296-347.

[16] Mochiyama, H., Suzuki. T., Kinematics and Dynamics of a Cable-Like Hyper-Flexible Manipulator, IEEE International Conference on Robotics and Automation, Vol. 3, No. 03CH37422, 2003, pp. 3672-3677.

[17] Yoon, H. S., Yi. B. J., A 4-DOF Flexible Continuum Robot Using a Spring Backbone, International Conference on Mechatronics and Automation, 2009, Aug 9, pp. 1249-1254.

[18] Tatlicioglu, E., Walker, I. D., and Dawson, D. M., New Dynamic Models for Planar Extensible Continuum Robot Manipulators, IEEE/RSJ International Conference on Intelligent Robots and Systems, 2007, Oct 29, pp. 1485-1490.

[19] George Thuruthel, T., et al., Control Strategies for Soft Robotic Manipulators: A Survey, Soft Robotics, Vol. 5, No. 2, 2018, pp. 149-163.

[20] Falkenhahn, V., et al, Model-Based Feedforward Position Control of Constant Curvature Continuum Robots Using Feedback Linearization, IEEE International Conference on Robotics and Automation (ICRA), 2015, May 26, pp. 762-767.

[21] Marchese, A.D., Tedrake, R., and Rus, D., Dynamics and Trajectory Optimization for A Soft Spatial Fluidic Elastomer Manipulator, The International Journal of Robotics Research, Vol. 35, No.8, 2016, pp. 1000-1019.

[22] Chikhaoui, M.T., et al., Toward Motion Coordination Control and Design Optimization for Dual-Arm Concentric Tube Continuum Robots, IEEE Robotics and Automation Letters, Vol. 3, No. 3, 2018, pp. 1793-1800.

[23] Li, M., et al., Model-Free Control for Continuum Robots Based on An Adaptive Kalman Filter, IEEE/ASME Transactions on Mechatronics, Vol. 23, No. 1, 2017, pp. 286-297.

[24] Esfandiar, H., Daneshmand, S., Closed Loop Control of The Planar Flexible Manipulator via Youla-Kucera parameterization, Journal of Mechanical Science and Technology, Vol. 27, No. 11, 2013, pp. 3243-3252.

[25] . Esfandiar, H., Daneshmand, S., and Kermani, R. D., On the Control of a Single Flexible Arm Robot via Youla-Kucera Parameterization, Robotica, Vol. 34, No. 1, 2016, pp. 150-172.

[26] Giri, N., Walker, I. D., Three Module Lumped Element Model of a Continuum Arm Section, IEEE/RSJ International Conference on Intelligent Robots and Systems, 2011, Sep 25, pp. 4060-4065.

[27] Bai, K., et al., Sliding Mode Nonlinear Disturbance Observer-Based Adaptive Back-Stepping Control of a Humanoid Robotic Dual Manipulator, Robotica, Vol. 36, No. 11, 2018, pp. 1728-1742.